THE JOURNAL OF PHYSICAL CHEMISTRY C

Article

pubs.acs.org/JPCC

Effects of Substitution with Donor–Acceptor Groups on the Properties of Tetraphenylethene Trimer: Aggregation-Induced Emission, Solvatochromism, and Mechanochromism

Xiao Yuan Shen,[†] Yi Jia Wang,[†] Engui Zhao,[‡] Wang Zhang Yuan,[‡] Yi Liu,[†] Ping Lu,[§] Anjun Qin,[†] Yuguang Ma,[§] Jing Zhi Sun,*[,†] and Ben Zhong Tang*[,†,‡]

[†]MoE Key Laboratory of Macromolecule Synthesis and Functionalization, Department of Polymer Science and Engineering, Zhejiang University, Hangzhou 310027, China

[‡]Department of Chemistry, Institute of Molecular Functional Materials, Institute for Advanced Study, The Hong Kong University of Science & Technology, Clear Water Bay, Kowloon, Hong Kong, China

[§]State Key Lab Supramolecular Structure & Materials, Jilin University, Changchun 130012, China

Supporting Information

ABSTRACT: Luminescent materials with aggregation-induced emission (AIE) property have attracted considerable interests for their promising applications in light-emitting and display devices and fluorescent probes for chemo- and biosensors. Tetraphenylethene (TPE) derivatives are the most attractive species for their notable AIE performance, facile synthesis, and flexible structure modification. To study the effects of donor and acceptor substitutions and extend the applications of TPE-based materials, three TPE kindred, TTPE, BTPEFN, and BATPEFN, are employed. TTPE film displays efficient green fluorescence (λ_{em} = 494 nm, Φ_F = 100%), evident AIE characteristic (α_{AIE} = 154), and reversible mechanochromism by grinding-fuming: from blue (λ_{em} = 472 nm) to green emission (λ_{em} = 505 nm). Replacing two phenyls by two cyano (A) groups on the central TPE moiety derives BTPEFN, whose film shows efficient orange fluorescence (λ_{em} = 575 nm, Φ_F = 100%) and evident AIE (α_{AIE} = 13). The mechanochromic behavior of BTPEFN (from yellow to orange emission, λ_{em} from 541 to 563 nm) is reversible by repeating both the grinding-fuming and grinding-annealing processes. The cyano groups bestow BTPEFN with evident intramolecular charge transfer (ICT) property, the emission color can be tuned from green to red-orange by changing solvent from hexane to THF, while the emission of TTPE shows much less response to solvent polarity. Cyanos also endow BTPEFN with better self-assemble ability in proper conditions, and the obtained regular microribbons emit bright green fluorescence. Further decoration of BTPEFN with *N*,*N*-diethyamino (D) groups results in BATPEFN. Due to the cooperative effects of D and A groups, BATPEFN shows dramatic red-shifted fluorescence (λ_{em} = 713 nm), evident ICT process, and enhanced solvatochromism (from red to infrared).

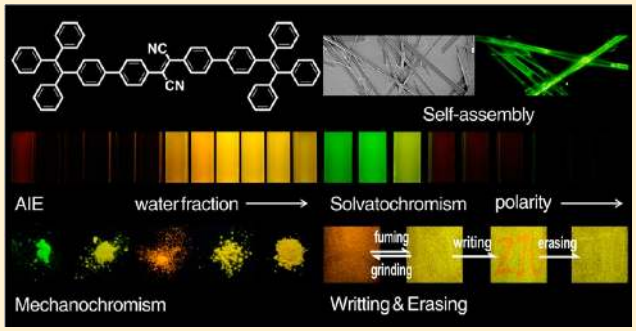

INTRODUCTION

Intensive efforts have been devoted to the development of organic photonic/electronic materials for their potential application in display, energy-efficient lighting, light harvest devices, and fluorescent sensors.[1−4] To meet these demands, efficient luminescent materials covering full RGB colors and the infrared region are highly necessary. Materials scientists mainly use two strategies to tune the luminescence wavelength by either changing the electronic structure of the conjugated system or introducing different dopants into the host materials.[5] In principle, it is the ultimate approach to achieve red-shifted luminescence through enlarging effective conjugation of the luminogens. However, many extended π-systems become weakly emissive when they are in solid or aggregation states despite being strongly emissive in dilute solutions. This effect is referred to as the infamous aggregation caused emission quenching (ACQ).[6] Dopant molecules are prone to aggregate formation because of the robust intermolecular interactions. Consequently, the doping systems are difficult to control due to the critical effective doping range and low optimum doping concentration.[7] To circumvent the ACQ effect and concentration quenching, researchers have developed various chemical and physical methods (e.g., attachment of branched chains or bulky cyclics, blending with polymers with high glass transition temperature and high transparency), but obtained limited success.[8−10] In thermodynamic principle, aggregate formation is an intrinsic process in the condensed phase, it seems that realizing luminescent organic solids with

Received: November 17, 2012
Revised: March 15, 2013
Published: March 19, 2013

   dx.doi.org/10.1021/jp311360p | J. Phys. Chem. C 2013, 117, 7334−7347

Scheme 1. Synthetic Routes to TTPE, BTPEFN, and BATPEFN

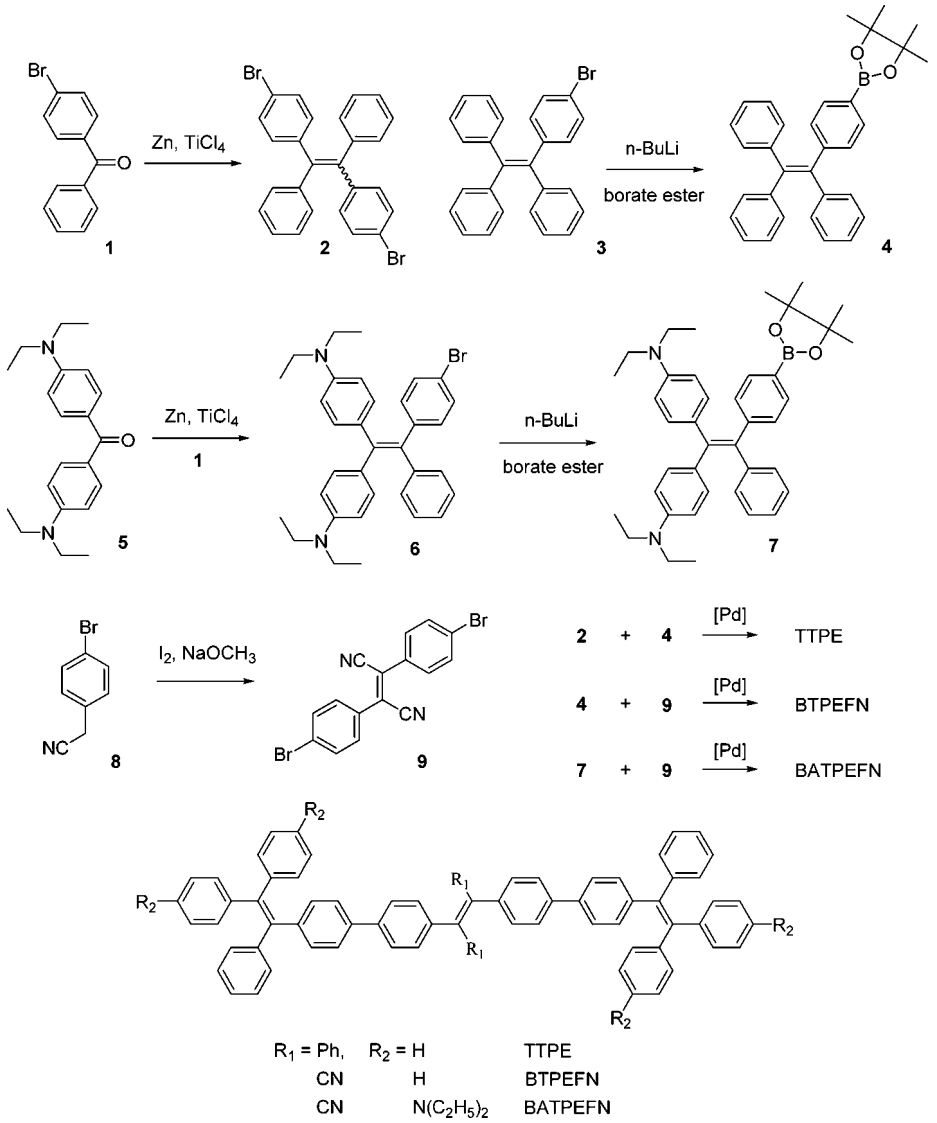

high quantum efficiency and long-term stability is an infeasible task.

The report of aggregation-induced emission (AIE) phenomenon gave a hint to end the dilemma. It was found that 1-methyl-1,2,3,4,5-pentaphenylsilole was faintly emissive in acetonitrile solution, but became strongly luminescent in aggregation or solid states.[11] This phenomenon is mainly ascribed to the restriction of intramolecular rotations (RIR) process: the nonluminescence of silole in solution is attributed to the active intramolecular rotations of multiple phenyl rings on its periphery, while the strong emission in the solid state is caused by the restriction of intramolecular rotations of those phenyl rings.[12] Based on the understanding of the mechanism, a growing number of molecules with AIE properties have been developed.[13−17]

Among these AIE systems, tetraphenylethene (TPE) and its derivatives have been put into the limelight by researchers for their simple synthetic routes and notable AIE performance.[18−34] A number of TPE-based derivatives have been synthesized. Nevertheless, there is still huge space to modify the structure and to develop TPE-based advanced functional materials. For example, most of the TPE-containing luminogens are blue or green emitting materials but only very few are red emitting ones,[21−23] which will find applications in many areas such as full-color organic light emitting diodes and bioimaging. In principle, red-shifted emission comes from a narrowed energy-gap, which can be realized by two strategies. One is by extending the π-conjugation system (mainly to drive up the highest occupied molecular orbital, or HOMO) such as those observed for large planar conjugated molecules.[35,36] And the other is by introducing D and A groups into a conjugated luminogen to concomitantly drive up the HOMO and pull down the lowest unoccupied molecular orbital or LUMO.[37] The latter has been successfully observed for a few long-wavelength AIE-active molecules such as 1,1-dimethyl-2,5-bis(4′-diphenylaminophenyl)-3,4-diphenylsilole (DMTPS-DPA), 1,1-dimethyl-2,5-bis(4′-benzylidenemalononitrile)-3,4-diphenylsilole (DMTPS-DCV),[38,39] and 2-(4-bromophenyl)-3-(4′-(dimethylamino)biphenyl-4-yl)fumaronitrile (BDABFN),[40] and we predict that this strategy will also work well in red-shifting the fluorescence of the TPE derivatives.

Moreover, TPE and its derivatives are composed of an ethenyl core and multiple rotational phenyl rings. Due to the steric repulsion between the adjacent phenyls, these molecules

dx.doi.org/10.1021/jp311360p | J. Phys. Chem. C 2013, 117, 7334−7347

Table 1. Optical and Electronic Properties of TTPE, BTPEFN, and BATPEFN[a]

		λ_{em} (nm)							
compd	λ_{abs} (nm)	soln (Φ_F)	aggr (Φ_F)	film (Φ_F)	E_g (eV)	HOMO (eV)	LUMO (eV)	T_m (°C)	T_d (°C)
TTPE	344	504 (0.3)	495 (46.2)	494 (100)	3.08	−5.40	−2.32	337	430
BTPEFN	399	590 (3.4)	565 (44.2)	575 (100)	2.66	−5.29	−2.63	247	456
BATPEFN	469	n.d.	n.d.	713 (0.01)	2.15	−4.75	−2.60	n.d.	325

[a]Abbreviation: λ_{abs} = absorption maximum, λ_{em} = emission maximum, Φ_F = fluorescence quantum yield (%) in dilute THF solution (soln), THF/water mixture with 80% (TTPE) or 90% (BTPEFN) water fraction (aggr) estimated by 9,10-quinine sulfate (54% in 0.1 N sulfuric acid) or Rhodamine B (70% in ethanol), thin film (film) determined by a calibrated intergrating sphere, E_g = energy gap calculated from the onset absorption wavelength, HOMO = the highest occupied molecular orbital determined by cyclic voltammetry, LUMO = the lowest unoccupied molecular orbital deduced from E_g and HOMO, T_d = temperature for 5% weight loss, T_m = melting temperature recorded by differential scanning calorimetry, and n.d. = not detectable (signal is too weak to be accurately determined).

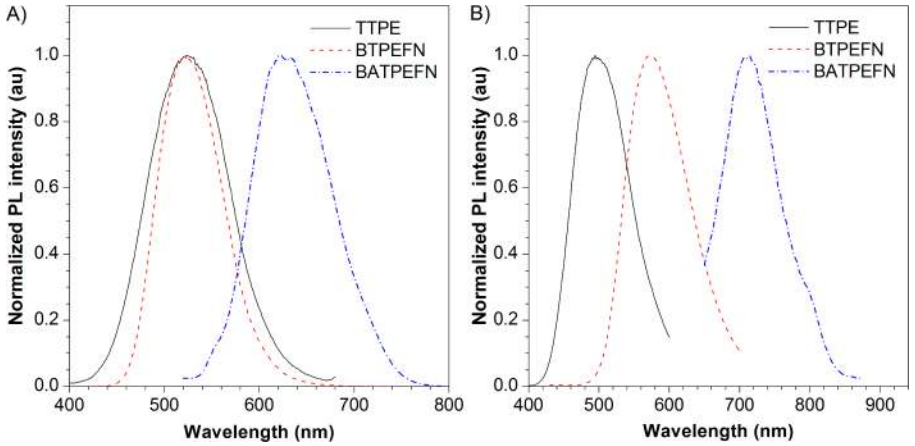

Figure 1. (A) PL spectra of TTPE, BTPEFN, and BATPEFN in the dilute hexane solution (concentration: 10 μM). (B) Normalized PL spectra of their films on quartz plate, excited on their absorption maxima (λ_{abs}).

have to take a nonplanar configuration. As a result, there is only a little intermolecular $\pi-\pi$ interaction possessed in their solids. The existence of multiple rotational phenyls, nonplanar shape, and weak $\pi-\pi$ interaction indicates that TPEs in condensed states may have loose molecular packing and good structural transformability. Indeed, in quite a few TPE derivatives, especially those containing electron donor and/or acceptor moieties, piezo-/mechano-, vapo-, solvato-, and thermochromism have been observed.[18,24] In a recent work, we have shown that, by directly attaching two triazolyl moieties onto two phenyls of TPE, the derived molecule displays weak solvatochromic and mechanofluorochromic behaviors.[18] In this case, the electron deficient or acceptor property of the triazolyl plays a key role. Considering that triazolyl is only a moderate electron acceptor, modification of TPE with stronger electron acceptors and/or donors must bestow the derivatives with more pronounced solvatochromic and mechanofluorochromic effects, and these derivatives may exhibit higher sensitivity and larger responsibility to external stimuli.

In this paper, we demonstrate a systematic study of the effects of substitution with electron donor (D) and/or electron acceptor (A) groups on the properties of a TPE trimer. As shown in Scheme 1, three molecules (TTPE, BTPEFN, and BATPEFN) are synthesized and employed for the comparative and systematic study. TTPE, BTPEFN, and BATPEFN stand for 1,2-diphenyl-1,2-bis(4′-(1,2,2-triphenylethenyl)biphenyl-4-yl)ethene, 2,3-bis(4′-(1,2,2-triphenylethenyl)biphenyl-4-yl)-fumaronitrile, and 2,3-bis(4′-(2,2-bis(4-(diethylamino)-phenyl)-1-phenylethenyl)biphenyl-4-yl)fumaronitrile, respectively. In TTPE or the TPE trimer, there is neither electron donor (D) nor electron acceptor (A) groups. In BTPEFN, the fumaronitrile group containing two cyano functionalities serves as representative A-type moieties. And in BATPEFN, the fumaronitrile and *N*,*N*-diethylamino groups play the roles of A- and D-moieties, respectively. Among these three molecules, BTPEFN and BATPEFN are first synthesized. TTPE was reported in our very recent work.[41] Here we use it as a reference and meanwhile we report some of its interesting novel properties together with the other two molecules so as to comprehensively elucidate the relationship between molecular structure and property.

RESULTS AND DISCUSSION

Synthesis. The synthetic routes to the TPE derivatives (TTPE, BTPEFN, and BATPEFN) are shown in Scheme 1. The experiment details and structure characterization data are described in the Experimental Section and the Supporting Information (SI). In brief, the target molecules are derived from the coupling of TPEs (**2**, **4**, **7**) and bis(4-bromophenyl)-fumaronitrile (**9**) under typical Suzuki reaction conditions with satisfactory yields.

All three of the compounds have good solubility in common organic solvents such as THF, chloroform, and toluene, but are insoluble in protic solvents such as water and methanol. The final products have been carefully purified and fully characterized by NMR, elemental analysis, and high resolution mass spectroscopies (SI, Figures S1−S3). Both TTPE and BATPEFN also passed the elemental analysis. But BTPEFN gave unsatisfactory results. This could be ascribed to the existence of wrapped solvent molecules which are difficult to

dx.doi.org/10.1021/jp311360p | J. Phys. Chem. C 2013, 117, 7334−7347

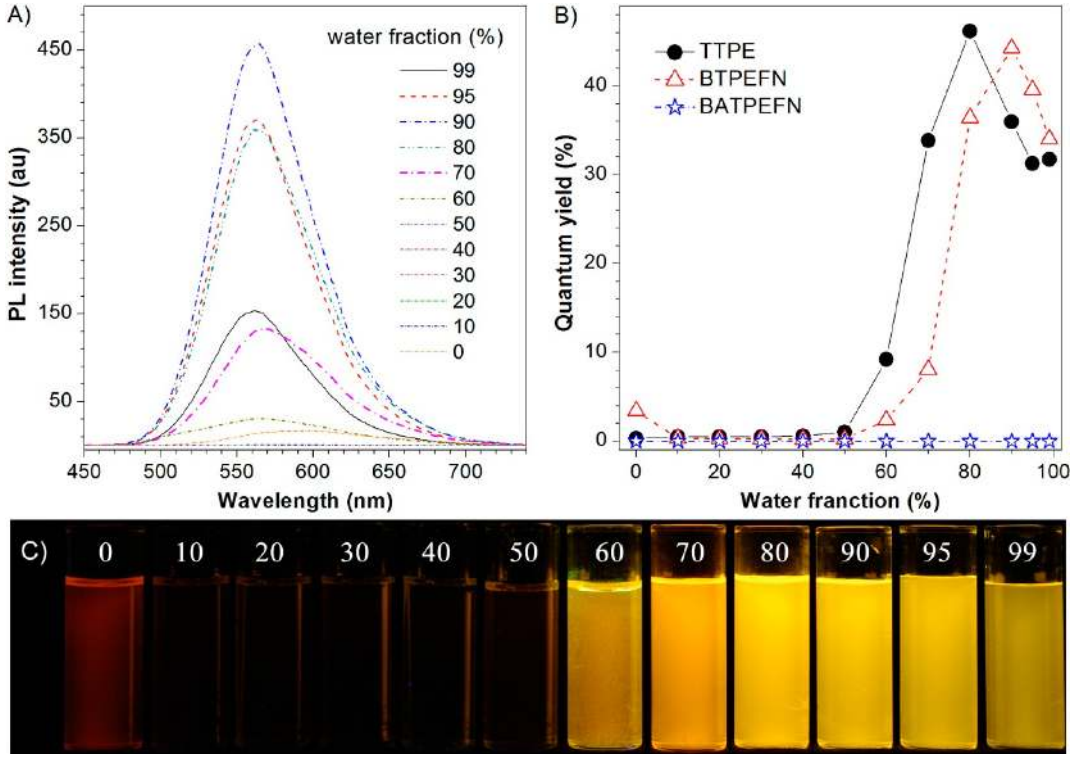

Figure 2. (A) PL spectra of BTPEFN in the THF/water mixtures. λ_{ex} = 399 nm. (B) Plots of fluorescence quantum yields (Φ_F) of TTPE, BTPEFN, and BATPEFN in the THF/water mixtures. (C) Photos taken under UV light of BTPEFN in the THF/water mixtures. The Φ_F values were estimated by using quinine sulfate in 0.1 N sulfuric acid (Φ_F = 54.6%) for TTPE, and Rhodamine B in ethanol (Φ_F = 70%) for BTPEFN and BATPEFN. Concentration: 10 μM.

remove under vacuum drying treatment. As a proof, the solvent endothermic peak at 131 °C can be found in the DSC diagram and it disappeared after the first heating and cooling cycle (SI, Figure S4). After thermal treatment at 160 °C for 10 h, acceptable elemental analysis data have been obtained (see the Experimental Section). Thermogravimetric analysis (TGA) and differential scanning calorimetry (DSC) results indicate that both TTPE and BTPEFN hold high melt points with T_m at 337 and 247 °C (SI, Figure S4), respectively, and high thermal stability with T_d at 430 and 456 °C, respectively (SI, Figure S5), where T_d corresponds to the temperature at which the compound lost 5% of its original weight. These data indicate that TTPE and BTPEFN have higher thermal treating tolerance than either the TPE derivatives, e.g., TPE (T_m = 222 °C, T_d = 224 °C) and bis(tetraphenylethene) (BTPE) (T_m = 290 °C, T_d = 368 °C), or the silole derivatives, e.g., 1,1,2,3,4,5-hexaphenylsilole (HPS) (T_m =186 °C, T_d = 351 °C), according to literature.[42] For BATPEFN, the introduction of the *N*,*N*-diethylamino groups is responsible for slightly lowered T_d (325 °C). The compound may have decomposed before T_d, thus T_m is absent on its DSC curve. The excellent thermal stability and good solubility in common solvents make these TPE derivatives suitable for the potential device applications and solution process.

Optical Properties. Absorption spectra of three molecules in dilute THF solution are shown in Figure S6 (SI). The absorption maximum (λ_{abs}) of TTPE, BTPEFN, and BATPEFN appears at 344, 399, and 469 nm (Table 1), respectively. Upon excitation, both TTPE and BATPEFN are nearly nonemissive, while BTPEFN exhibits a weak orange emission in dilute THF solution. In dilute hexane solution, TTPE and BTPEFN emit green photoluminescence (PL) with a maximum (λ_{em}) at around 524 nm, and BATPEFN emits red PL with a maximum at 623 nm (Figure 1A). When spin-coating on quartz plates, amorphous solid films are obtained and the TTPE film emits bright bluish green PL with λ_{em} at 494 nm (Figure 1B). According to literature, the emission peak for the amorphous film of TPE and BTPE is recorded at 503 and 499 nm, respectively.[43,44] These data indicate that it has no effect on red-shifting the PL features by simply extending the chain length from TPE monomer to dimer (BTPE) and trimer (TTPE). This observation is quite distinct from all known conjugated polymers, for which the PL feature displays an unceasing monotonous red-shift with the increasing of repeat units until the full effective conjugation length is reached. The reason for the unique fluorescent behavior of the TPE-oligomers can be tentatively ascribed to the molecular structure of TPE derivatives. The molecules have highly twisted conformations (or nonplanar configurations), thus the adjacent TPE units are not in good conjugation state and the PL feature is mainly determined by a single TPE unit regardless to the number of repeat units in an oligomer chain. Moreover, we have demonstrated that it has little effect on the PL features by changing the linking mode (linked directly, or linked via double and triple bonds) between the TPE moieties.[41] Consequently, other strategies have to be adopted in the molecular design in order to shift the PL features of TPE oligomers.

As we have anticipated, introducing D and/or A groups to the TPE derivatives can prominently help to red-shift the PL spectrum. When two phenyl groups on the central TPE moiety of TTPE are replaced by two cyano ones, the derived fumaronitrile motif plays the role of electron acceptor, and the compound BTPEFN becomes a typical π−A−π structure. As shown in Figure 1B, the solid film of BTPEFN exhibits an

dx.doi.org/10.1021/jp311360p | J. Phys. Chem. C 2013, 117, 7334−7347

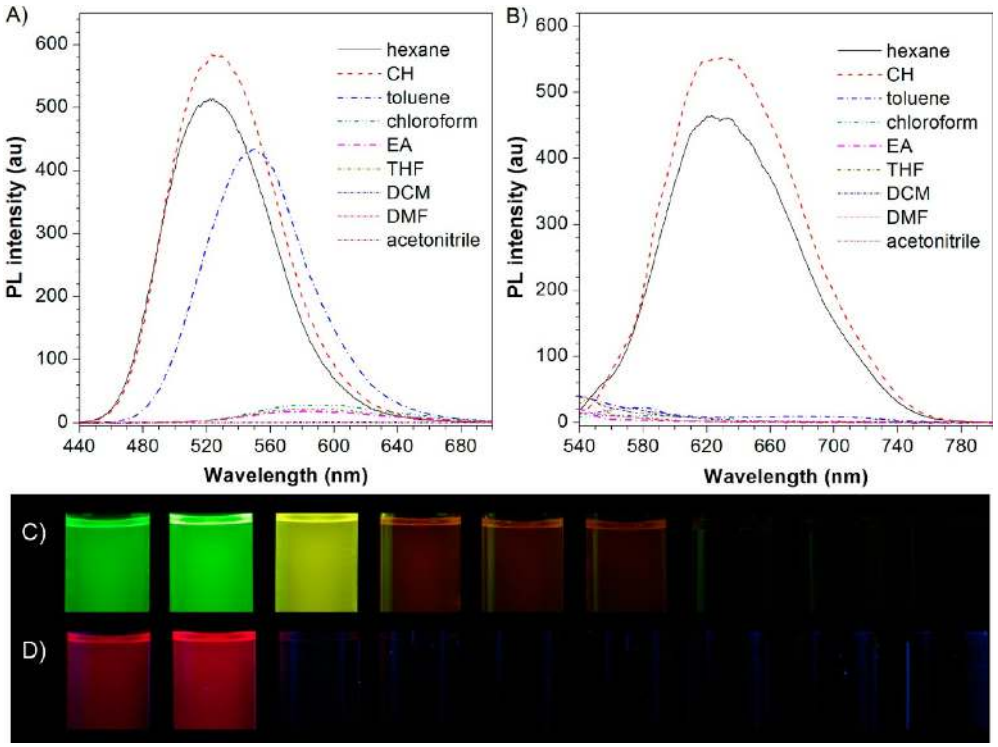

Figure 3. PL spectra of (A) BTPEFN and (B) BATPEFN in different solvents. Photographs of (C) BTPEFN and (D) BATPEFN taken under UV illumination in different solvents, from left to right: hexane, cyclohexane, toluene, chloroform, ethyl acetate, THF, DCM, DMF, and acetonitrile. The solutions were excited at their absorption maxima. Concentration: 10 μM.

intensive orange emission peaked at 575 nm, about an 80 nm red-shift in comparison with the emission peak of amorphous TTPE film. When four electron donors (e.g., *N*,*N*-diethylamino groups) are attached onto the peripheral phenyls of BTPEFN, BATPEFN has been derived and it has a typical D−π−A−π−D structure. The PL feature for the solid film of BATPEFN is further red-shifted to the near-infrared region and the λ_{em} appears at 713 nm, about a 220 nm red-shift in comparison with the emission peak of amorphous TTPE film.

From the absorption and emission spectra, the Stokes' shifts of TTPE, BTPEFN, and BATPEFN are calculated to be 150, 176, and 244 nm, respectively. Taking TTPE as the reference, the above data indicate that the intramolecular charge transfer (ICT) property for BTPEFN and BATPEFN is weak and strong, respectively. The fluorescence quantum efficiencies of TTPE, BTPEFN, and BATPEFN solid films (Φ_F) are 100%, 100%, and 0.01%, respectively. The drastically decreased Φ_F value for BATPEFN can be ascribed to the strong ICT process and dipole−dipole interaction between the molecules.

In previous works, we demonstrated that TPE, BTPE, and TTPE derivatives were AIE active molecules.[41−44] To examine whether BTPEFN and BATPEFN are AIE active molecules or not, TTPE, THF, and water were used as a model compound, solvent, and nonsolvent, respectively. As revealed by data and the photographs in Figures 2 and S7 (SI), the three compounds TTPE, BTPEFN, and BATPEFN display three distinct fluorescent behaviors in THF/water mixture solutions with different water fractions (f_w, the volume percentage of water in THF/water mixtures). For TTPE, it shows typical AIE behavior (Figures 2B and S7, SI) in comparison with its analogues of TPE and BTPE. In dilute THF solution, TTPE is nearly nonemissive and its Φ_F is only 0.3%. In THF/water mixtures with low water fraction ($f_w \leq 50\%$), the fluorescence intensity and quantum efficiency remain unchanged. When f_w is higher than 50%, the solutions emit bright bluish green light with λ_{em} at 495 nm upon photoexcitation. The pronounced fluorescence enhancement phenomenon can be interpreted as the aggregation of TTPE molecules at higher f_w values. According to the above-mentioned RIR mechanism, when the TTPE is dissolved in THF or THF/water mixtures with $f_w \leq$ 50%, the active intramolecular rotations of multiple phenyl rings exhaust the energy of the excited states and result in fluorescence quenching. When more water, a nonsolvent for TTPE, is added into the solution, TTPE molecules tend to form aggregates, thus the intramolecular rotations of the phenyl rings are restricted and the excited states decay to the corresponding ground states through irradiative channels thereby strong emission is recorded. At the f_w of 80%, a maximum Φ_F of 46.2% has been recorded, and the corresponding amplification factor α_{AIE} ($\alpha_{AIE} = \Phi_{F,\,aggr}/\Phi_{F,\,soln}$) is as high as 154.

BTPEFN displays different fluorescent behaviors from TTPE in THF/water mixture solutions with different f_w values. In THF, or f_w = 0, BTPEFN emits red-orange fluorescence and the λ_{em} appears at 590 nm, but the intensity is weak and Φ_F is only 3.4% (Figure 2A,B). When the proper amount of water is added into THF solution, the emission peak disappears due to the increase in the solvent polarity. The fluorescence quenching is ascribed to the ICT effect in polar solvent for BTPEFN with a π−A−π structure. When f_w is above 60%, the PL is recovered and the intensity increases quickly. At the same time, the λ_{em} gradually blue-shifts from 590 to 574 nm, and the emission color changed from red-orange to yellow (Figure 2C). These observations can be interpreted as following: When a large amount of nonsolvent (f_w > 60%) exists in the mixture, BTPEFN molecules tend to aggregate, inside which the

dx.doi.org/10.1021/jp311360p | J. Phys. Chem. C 2013, 117, 7334−7347

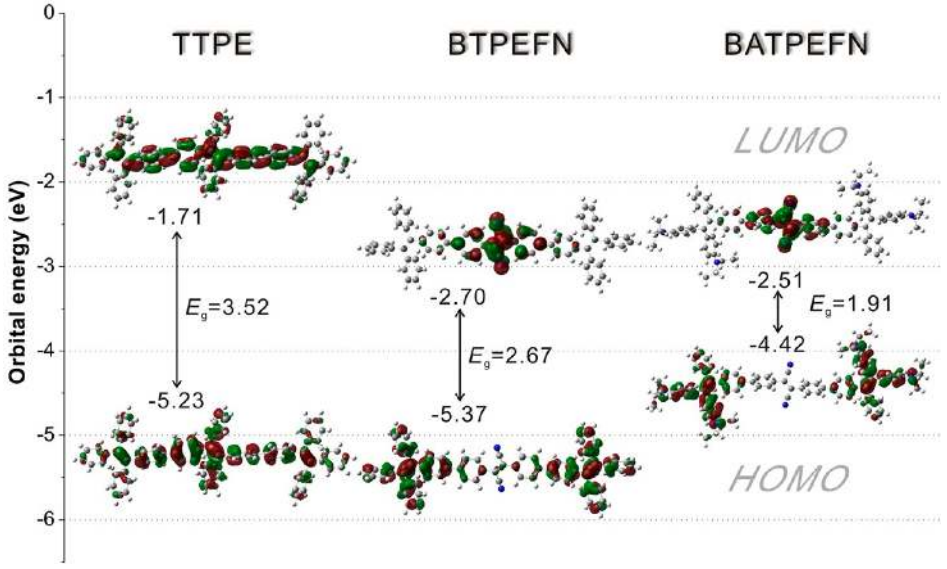

Figure 4. Energy levels of HOMO and LUMO, energy gaps, and electron cloud distributions of TTPE, BTPEFN, and BATPEFN molecules calculated by the B3LYP/6-31G(d) program.

encapsulated BTPEFN molecules locate in a nonpolar environment and the ICT process is limited, thus the fluorescence is recovered. Meanwhile, the fluorescence feature of the aggregates blue-shifts to the same region as the solid film of BTPEFN (Figure 1B). When f_w is higher than 95%, the PL intensity decreases. This phenomenon is reasonable that at high water fraction ($f_w \geq 95\%$), the hydrophobic BTPEFN molecules are apt to aggregate into larger particles and precipitate quickly. This process leads to the decrease of fluorescent species in the system and lowers the fluorescence intensity and apparent quantum efficiency. A direct evidence of particle formation is the level-off tails in the absorption spectra of the mixtures with high f_w values (SI, Figure S8), which is known as the Mie effect.[45] Since Φ_F of BTPEFN is 3.4% and 44.2% in pure THF and in THF/water mixture at f_w = 90% (Figure 2B), the α_{AIE} of BTPEFN is about 13.

For BATPEFN, the D−π−A−π−D structure renders it a very strong ICT process in polar solvents and heavy fluorescence quenching effect. No AIE behavior has been observed although we have tried a few different solvent/nonsolvent systems such as THF/water, THF/methanol, and dichloromethane (DCM)/hexane.

Solvatochromic Effect. Introduction of electron donor and/or acceptor groups to a fluorogen can endue it with not only the ICT property, but also with the solvatochromic effect. Experimental data indicate that both BTPEFN and BATPEFN exhibit pronounced solvatochromic performance. As shown in Figure 3A, for BTPEFN, an evident red-shift of λ_{em} from 524 to 599 nm accompanied by a notable decrease in intensity is observed when the solvent changes from apolar (e.g., hexane) to highly polar ones (e.g., acetonitrile). In contrast, the λ_{abs} appears at around 400 nm and shows only a small shift from 405 to 390 nm (SI, Figure S9A). Figure 3C displays the fluorescence images of the corresponding solutions. Under UV light, BTPEFN emits strong green light in hexane and cyclohexane, bright yellow light in toluene, and weak red-orange solvents in chloroform, ethyl acetate, and THF. In more polar solvents such as DCM, DMF, and acetonitrile, the emission becomes very weak and the peak shifts further to the red region. As shown by Figure 3D, when excited by UV light, BATPEFN emits red light in apolar solvents such as hexane and cyclohexane. Whereas in the quasi-apolar solvent toluene, the emission becomes deep red and the intensity becomes lower. In polar solvents such as chloroform, THF, and acetonitrile, the emission is nearly invisible by the naked eye. The changes in the emission features are quantitatively evaluated by fluorescence spectroscopy (Figure 3B). A large red shift of λ_{em} from 623 to 687 nm is recorded with the change in solvent polarity. Simultaneously, the emissions become weaker. In contrast, the UV−vis absorption spectra of these BATPEFN solutions display little changes (λ_{abs} = 470 nm) with the change in solvent polarity (SI, Figure S9B). We also tested the solvent effect of TTPE. It emits strong green light with a peak at 525 nm in apolar solvent (hexane and cyclohexane), but in polar solvents (including chloroform, ethyl acetate, THF, DCM, acetonitrile, and DMF), the emission becomes much weaker and the λ_{em} blue-shifts to about 500 nm (SI, Figure S10). Similar to that observed for BTPEFN and BATPEFN, the absorption features also show little change with the change of solvent polarity.

$$\Delta\upsilon \equiv \upsilon_{ab} - \upsilon_{em} = \frac{2\Delta f}{hca^3}(\mu_e - \mu_g)^2 + \text{constant} \quad (1)$$

$$\Delta f = f(\varepsilon) - f(n^2) \approx \frac{\varepsilon - 1}{2\varepsilon + 1} - \frac{n^2 - 1}{2n^2 + 1} \quad (2)$$

The effects of solvents on the emission features can be further evaluated by the relationship between the solvent polarity parameter (Δf) and Stokes shift of the absorption and emission maxima (Lippert−Mataga equation, eqs 1 and 2),[46,47] where, $\Delta\upsilon$ is the Stokes shift, h is the Planck constant, c is the speed of light, a is the Onsager cavity radius, μ_e and μ_g refer to the dipolar moments in the excited and ground states, and ε and n are the dielectric constant and refractive index of the solvent, respectively. The experimental data of BTPEFN, BATPEFN, and TTPE are summarized in Table S1 (SI). Both BTPEFN and BATPEFN show positive solvatochromism. Their emission peaks red-shift and quantum yields decrease gradually with the increasing of Δf. From the plots of $\Delta\upsilon - \Delta f$, we can find that the slopes of the fitting line for BTPEFN and

dx.doi.org/10.1021/jp311360p | J. Phys. Chem. C 2013, 117, 7334−7347

BATPEFN are as high as 9531 and 45788, exhibiting significant solvatochromism effect (SI, Figure S11). Whereas, the fitting line for TTPE is negative with a small slope of −882, showing a slight negative solvent effect, i.e., as the polarity of the solvent increases, the emission of the TTPE solution blue shifts. This may be because the equilibrium set between TTPE and solvent molecule reduces more energy in the ground state than in the exited state.[48] Another possible explanation is that TTPE molecules exhibit more twisted conformation in polar solvents than in apolar ones.

Electronic Structure. To obtain a better understanding of the optical properties and solvent effects of these three TPE derivatives, we performed theoretical calculations on their energy levels by using the density functional theory (DFT) method at B3LYP/6-31G(d) basis in the Gaussian 03 E01 package.[49] The simulation results including the optimized molecular configuration, energy levels, and electron distributions of the HOMO and LUMO of *trans*-TTPE, BTPEFN, and BATPEFN are shown in Figure 4. According to our previous work,[41] the calculated HOMO and LUMO of the *cis* and *trans* isomers are almost the same; here we employ the *trans* one as a representative. For *trans*-TTPE, the electron clouds of both the HOMO and LUMO are distributed evenly along the long axis of the molecule. This result suggests that, on one hand, the optical transition from LUMO to HOMO is a direct one, which offers a high fluorescent efficiency to TTPE molecules; on the other hand, the TTPE molecule has no ICT process, which is consistent with the observed optical property (Figure 1). In sharp contrast, when a strong electron acceptor or cyano groups is attached to the backbone of TTPE, the HOMO and LUMO of BTPEFN are mainly located on the terminal TPE units and central fumaronitrile core, respectively. As a result, an evident ICT from the peripheral TPEs to the central fumaronitrile core is anticipated. This process has been confirmed by the fluorescent behaviors of BTPEFN in solvents with different polarity and in THF/water mixtures with different water fractions (Figures 2 and 3). When strong electron donors (i.e., *N*,*N*-diethylamino groups) are attached to the phenyls of the peripheral TPEs, it can be found that the HOMO and LUMO of BATPEFN localize separately and completely on two terminal TPE units and central fumaronitrile core, respectively. Such an orbital distribution indicates that the BATPEFN molecule has a stronger ICT tendency, which may induce the consumingly quenched fluorescence of BATPEFN in polar solvents.

The calculated HOMO levels of TTPE, BTPEFN, and BATPEFN are −5.23, −5.37, and −4.42 eV, respectively (Figure 4). The HOMO levels of organic compounds can also be estimated by using the cyclic voltammogram (CV) method. As demonstrated in Figure S12 (SI), the CV curves of TTPE, BTPEFN, and BATPEFN show oxidation onset potentials at 1.00, 0.89, and 0.35 V, respectively. The HOMO levels of these three compounds are −5.40, −5.29, and −4.75 eV, respectively, according to the calculation formulism reported in the literature.[50] Moreover, the theoretical energy gaps for TTPE, BTPEFN, and BATPEFN are 3.52, 2.67, and 1.91 eV, respectively; These parameters estimated by UV−vis spectra corresponding to TTPE, BTPEFN, and BATPEFN are 3.08, 2.66, and 2.15 eV, respectively. The theoretical data are quite consistent with the experimentally measured results both in tendency and absolute values. Accordingly, the electronic structure (HOMO, LUMO levels, and energy gap) and the opto-electronic properties (emission color and intensity, ICT process) of the TPE derivatives can be tuned by rational molecular design.

Self-Assembly. The calculation results and the experimentally observed AIE phenomenon have shown that TPE derivatives adopt twisted conformations. The propeller shape disturbs intermolecular $\pi-\pi$ stacking. Although we knew that perylene bisimides modified by TPE moieties could self-assemble into ordered microstructures, the robust $\pi-\pi$ interaction between the large planar cores still plays a helpful role in the self-assembling process.[22] Without large planar cores in TTPE, BTPEFN, and BATPEFN molecules, dipole−dipole interaction, rather than $\pi-\pi$ interaction can also be utilized to achieve ordered self-assemblies. In fact, self-assembly has been commonly observed in cyano-substituted conjugated molecules.[51,52] And more recently, we found that *trans*-TPE derivative can form well-ordered microfibers when polar triazolyl moieties were introduced into the molecule.[18] Considering that BTPEFN and BATPEFN are both polar molecules, we expect that ordered microstructures can be obtained in proper conditions.

As described in optical properties, BTPEFN molecules tend to aggregate in THF/water mixture solutions with high f_w values. After standing for 24 h, precipitate was formed in the THF/water mixture with f_w = 50% and it emitted yellowish green light. The morphology of the precipitate was examined with a scanning electron microscope (SEM). As displayed in Figure 5A, numerous regular microribbons are observed, and

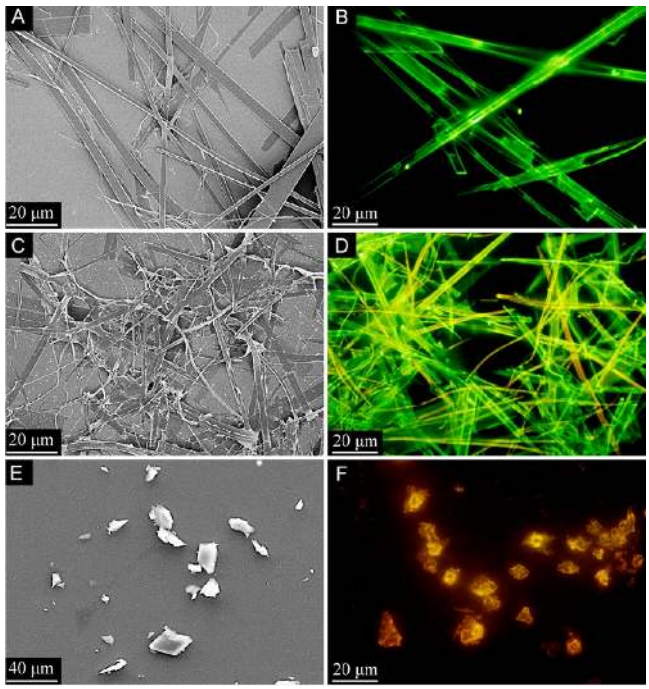

Figure 5. SEM (A, C, E) and fluorescence microscope (B, D, F) images of BTPEFN formed from THF/water mixtures. (A, B) f_w = 50%; (C, D) f_w = 60%; (E, F) f_w = 70%.

the typical length and diameter are hundreds of micrometers and several micrometers, respectively. When f_w increased to 60%, the precipitate formed more quickly. The sizes of the microribbons became smaller and the regularity of the morphology decreased concomitantly (Figure 5C). No ordered microstructures are observed when f_w is higher than 70% (Figure 5E).

dx.doi.org/10.1021/jp311360p | J. Phys. Chem. C 2013, 117, 7334−7347

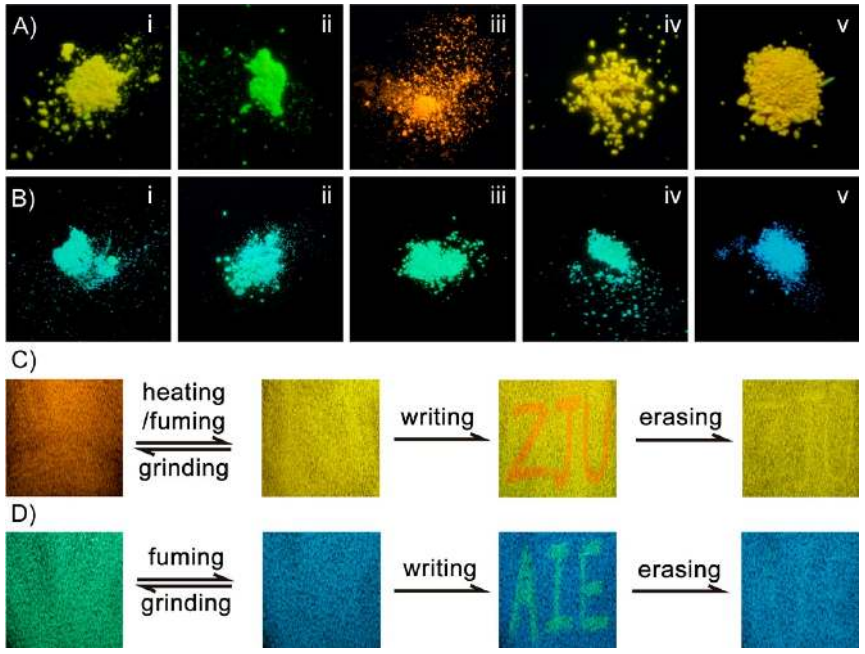

Figure 6. Photos of different solids for (A) BTPEFN and (B) TTPE: (i) aged powder, (ii) as-prepared powder, (iii) ground powder, (iv) after thermal annealing, and (v) fumed in DCM atmosphere taken under UV light (λ_{ex} = 365 nm). (C) BTPEFN and (D) TTPE are ground on filter papers, after initializing by heating or fuming process, the letters of "ZJU" were written on the BTPEFN "paper" and "AIE" on the TTPE "paper" with a spatula, and subsequently the papers were erased by thermal annealing (only BTPEFN) or vapor fuming (both BTPEFN and TTPE) (the letters "ZJU" and "AIE" becoming invisible under UV light).

Fluorescent microscopic images were also taken to investigate the morphology. The size and shape revealed by fluorescent microscopic images are consistent with that of SEM. Nevertheless, the emission colors of different structures are quite different: the large and regular microribbons emit yellowish green light (Figure 5B), while the thin and irregular microfibers emit yellow light (Figure 5D), and the featureless aggregates emit orange light (Figure 5F). The well-resoluble XRD pattern and the morphological observations for the precipitates obtained from a 50% THF/water mixture suggest that the yellowish green emitting microribbons are in microcrystalline state (SI, Figure S13). By comparing the emission color and the diffraction patterns between the disordered precipitate and ground powder (see the discussion in the part of Mechanochromism), we can assign the orange emitting entities to amorphous aggregates.

The differences in morphological observations, fluorescent microscopic images, and XRD patterns can be explained as follows. At f_w = 50%, BTPEFN has sufficient solubility in the THF/water mixture, the molecular aggregation process is slow, thus ordered assemblies or microcrystallines can be generated. When f_w is increased to 60%, the aggregation process is speeded up, and the size of the aggregate becomes smaller. Meanwhile, some of the molecules take a less ordered mode. Consequently, both yellowish green emitting and yellow emitting assemblies coexist in the precipitates. At higher f_w (≥70%), molecular aggregation is too fast to allow BTPEFN molecules to arrange in a well-defined packing mode, thus disordered yellow-orange solids have been obtained.

In comparison with BTPEFN, the structures generated by TTPE in THF/water mixtures are much smaller and irregular. For example, in a THF/water mixture with f_w = 60%, only nanofibers of diameter less than 100 nm and a length of several micrometers can be found in SEM images (SI, Figure S14A). At higher f_w (≥70%), irregularly shaped particles are formed in the THF/water mixture (SI, Figure S14C). Under UV light excitation (λ_{ex} = 365 nm), the nanofibers and particles display blue and green emission, respectively (SI, Figures S14B and S14D), and the blue emission is also related to the crystallization of TTPE, seeing the diffraction spots in the electron diffraction pattern of the aggregates of TTPE formed in 60% aqueous mixture (SI, Figure S15). Comparing the self-assembling performance of BTPEFN and TTPE, it can be concluded that the introduction of highly polar cyano groups into TPE derivatives is a salutary strategy for molecular design to enhance the intermolecular interactions and to create ordered assemblies from bulky molecules with highly twisted conformations.

Mechanochromism. Recently, a number of cyano-substituted fluorogens[53,54] and TPE derivatives[24,25,55] have been found to exhibit multiple stimuli-responsive fluorescence transitions in the solid state, such as piezo-/mechano-, vapo-, and thermochromism. This means their fluorescent behaviors can be changed in response to external pressure, volatiles, and temperature. With both cyano groups and TPE moieties, BTPEFN is greatly anticipated to be mechanochromic active.

BTPEFN is a yellow solid with bright yellow emission after running the column (Figure 6A-i). After being aged for months, the solid turns a light green and its emission blue-shifts from yellow to yellowish-green (Figure 6A-ii). By simply grinding the as-prepared solid of BTPEFN with a mortar and pestle, an orange powder with orange emission is obtained (Figure 6A-iii). From the PL spectra (Figure 7A) of the as-prepared and the ground solids, the former and the latter show emission peaks at 541 and 563 nm, respectively. This indicates that the grinding treatment has induced a spectral red-shift of 22 nm, and this is a typical mechanochromic phenomenon.

dx.doi.org/10.1021/jp311360p | J. Phys. Chem. C 2013, 117, 7334−7347

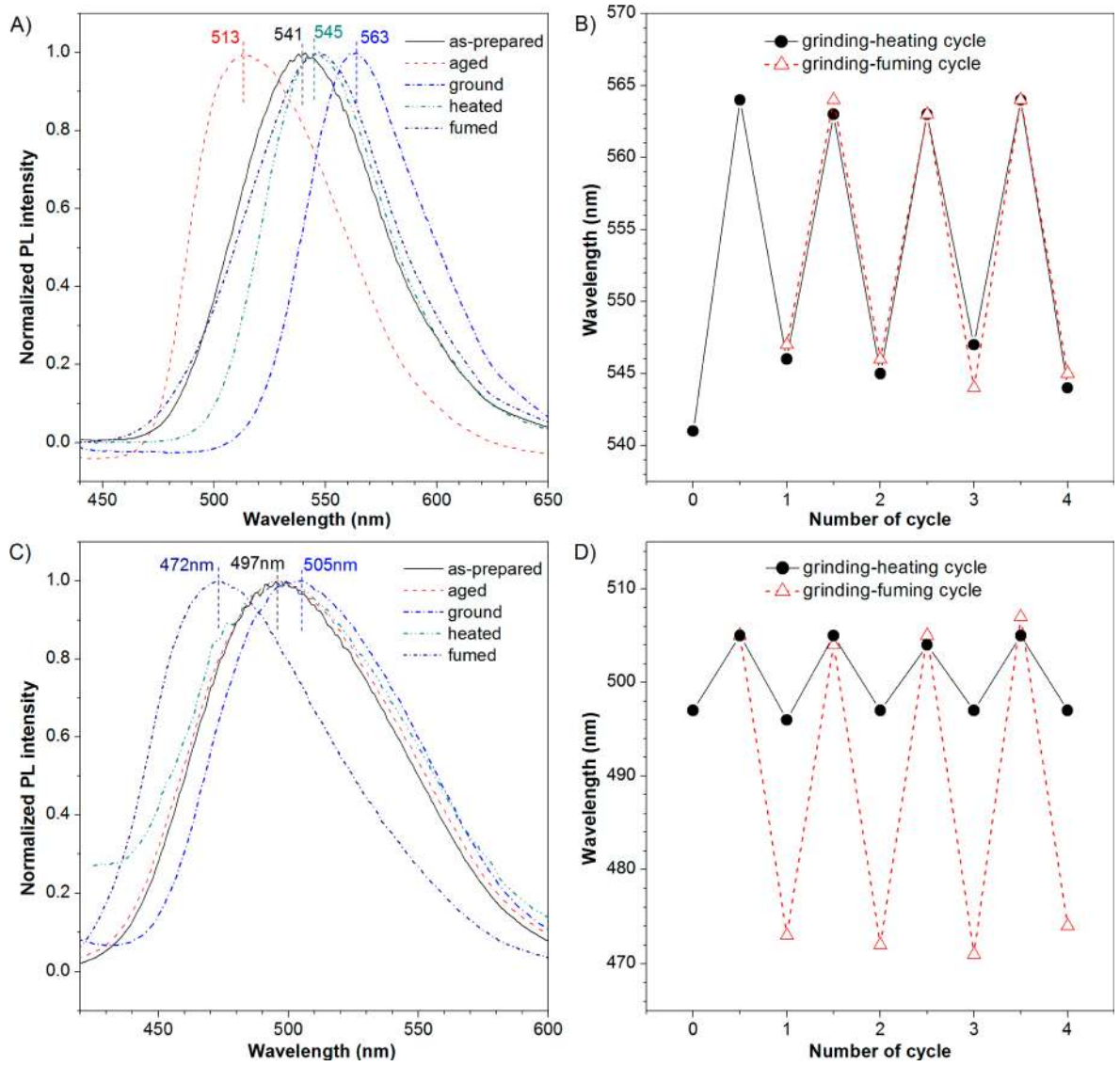

Figure 7. (A) The PL spectra of different solids for BTPEFN. λ_{ex} = 434 nm. (B) Switching of the solid-state fluorescence of BTPEFN by repeated grinding-heating process and grinding-fuming process. (C) The PL spectra of different solids for TTPE. λ_{ex} = 370 nm. (D) Switching of the solid-state fluorescence of TTPE by repeated grinding-heating process and grinding-fuming process.

A normal mechanochromic phenomenon usually shows reversible changes in color and emission. For application in sensors, ambient monitoring, or security inking, the reversibility of the transition is of great significance. To check the reversibility of the mechanochromic phenomenon observed for BTPEFN powder, we first treated the ground powder by thermal treatment. The annealing temperature is determined by the DSC data (SI, Figure S4). According to the DSC curves, without thermal annealing, the solid of BTPEFN has a weak transition at around 148 °C before its melting point. After thermal treatment, there is no thermal transition below a faint transition at about 205 °C and the melting point at about 230 °C. Moreover, the thermogravimetric analyzing results indicate the decomposition temperature of BTPEFN is 456 °C (SI, Figure S5). Thus we chose 160 °C as the temperature for sample treating. After thermal annealing at 160 °C for 10 min, the color and emission reverted to the original states (Figure 6A-iv). A set of four cycles of repeated grinding-heating processes is shown in Figure 7B. The results confirm that the mechanofluorochromic process is reversible. It is noted that the thermal annealing progress can be replaced by vapor fuming. When the ground solid was exposed to organic solvent vapor, such as DCM or THF, the color and emission were also recovered (Figure 6A-v).

To understand the mechanism of this mechanochromism, we carried out X-ray diffraction (XRD) measurements for these differently treated samples. According to the XRD data of the as-prepared BTPEFN solid (Figure 8, curve a), the diffraction pattern exhibits multiple strong and sharp diffraction peaks, implying that the sample is in the polymorphous and microcrystalline state. After being aged for months, the diffraction peaks became sharper and the baseline became smoother, indicating the microcrystallines grew larger and the defects in the crystals decreased (curve b). However, for the ground sample, most of the reflection peaks disappeared and only obtuse peaks at 25.7°, 24.8°, 20.5°, 18°, 11.6°, and 9.5° can be recognized (curve c), suggesting that the ordered state had been substantially demolished to the amorphous one. After annealing at 160 °C for 10 min, the diffraction pattern shows multiple strong and well-resolved diffraction peaks, manifesting

dx.doi.org/10.1021/jp311360p | J. Phys. Chem. C 2013, 117, 7334−7347

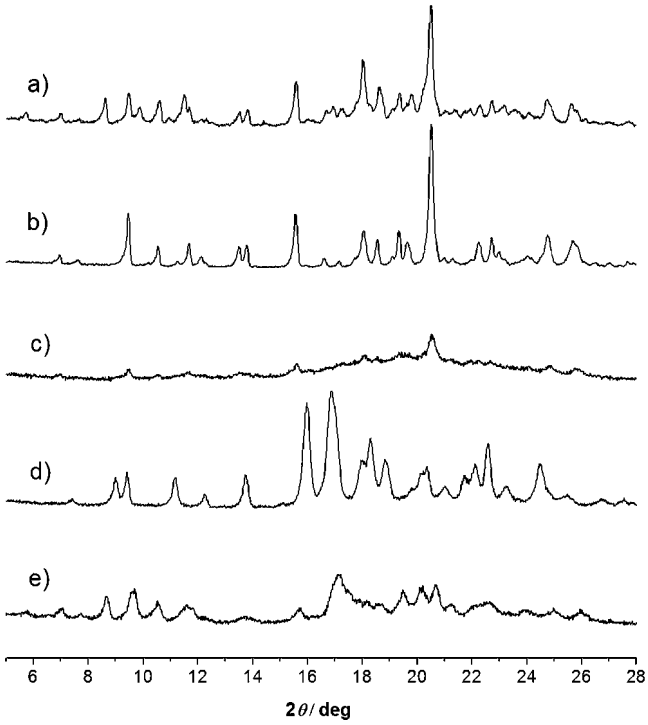

Figure 8. XRD patterns of BTPEFN solids: (a) as-prepared powder, (b) aged powder, (c) ground powder, (d) after thermal annealing, and (e) fumed with DCM.

that the amorphous ground sample has recrystallized into microcrystalline upon thermal treatment at elevated temperature. But by careful comparison of curve d with curve a, it can be seen that some of the reflection peaks appear in different 2θ values. For example, the peaks at 18.77°, 16.87°, 11.17°, and 8.98° on curve d cannot be found on curve a, indicating that polymorphs obtained by thermal treatment are not the same as the as-prepared BTPEFN solid. Elemental analysis data also indicate that thermal treating drives off the encapsulated solvent molecules. The diffraction pattern of the ground sample fumed by DCM vapor is largely similar to curves a and b, except for reflection peaks at 17.16° and 15.74°. This suggests that the polymorphs of the solvent fumed sample are similar to that of the as-prepared solid but dissimilar to the thermally treated sample (curve e). The XRD data demonstrate the mechanochromisms are attributed to the transformations between the polymorphous and amorphous states. This is a general mechanism for most mechanochromic compounds.[24,25,56]

We also examined the mechanofluorochromic behavior of TTPE solid, which was not reported in our previous work.[41] Both the as-prepared and aged samples of TTPE show bluish-green emission around 497 nm (Figure 6B-i ,ii). After grinding, the λ_{em} appears at 505 nm with only a small red shift of 8 nm (Figures 6B-iii and 7C). Although the emission could blue-shift back to 497 nm again by annealing at 200 °C for 20 min, the weak and broad XRD patterns (SI, Figure S16, curves a–d) of all the above samples indicate there is no polymorphous–amorphous transition during the grinding-heating process. However, upon exposure to DCM vapor, bright blue light emission is observed with a blue shift from 505 to 472 nm (Figure 6B-v). The intensive and well-resolved XRD pattern (SI, Figure S16, curve e) of fumed sample suggests that fuming with solvent converted the phases from amorphous to crystalline. Furthermore, this grinding-fuming fluorochromic process is also reversible (Figure 7D).

The mechanochromic behaviors for BTPEFN and TTPE reveal two different characteristics. First, the initial state of BTPEFN is polymorphous whereas TTPE is amorphous, suggesting a stronger crystallizability for BTPEFN in normal temperature. Second, the mechanochromsim of BTPEFN can be repeated by both the grinding-heating and grinding-fuming processes, while for TTPE, only the grinding-fuming process is taken into effect. This is reasonable because no cold crystallization peak is found in the low-temperature region of the DSC curve for TTPE (SI, Figure S4). These comparative experimental results demonstrate that the cyano groups in BTPEFN play a crucial role in the mechanochromism of TPE derivatives, as observed for other stimuli-responsive AIE compounds.[24,38,39]

It can be noted that both BTPEFN and TTPE possess reversible multistimuli-responsive fluorochromic properties, that is, they are a kind of smart material with numerous potential applications. Here is an example of such application (Figure 6C,D). When the compounds are ground onto filter papers, BTPEFN and TTPE emit orange and green light under UV light, respectively. After initializing by fuming (both BTPEFN and TTPE) or heating (only BTPEFN) treatments, the emissions of BTPEFN and TTPE "papers" turn yellow and blue. Then the letter "ZJU" is written on the BTPEFN "paper" and the letter "AIE" is written on the TTPE "paper" by gently scraping with a spatula. Under a hand-held UV lamp, the letter "ZJU" emits orange light and the letter "AIE" emits green light. The letter "ZJU" on the BTPEFN "paper" can be erased by either thermal annealing or vapor fuming treatment, while the letter "AIE" on the TTPE "paper" can be erased only by the vapor fuming procedure. Since the letters can be seen with UV light, but no apparent marks with daylight, BTPEFN and TTPE can be used as security inks, latent image developer, and other rewritable information storage systems.

CONCLUSION

In summary, we have demonstrated the molecular design, synthesis, and properties of three TPE derivatives (TTPE, BTPEFN, and BATPEFN). In combination with our previous research results, we have found that TTPE, similar to its analogues TPE and BTPE, shows highly efficient bluish green fluorescence ($\lambda_{em,\ TTPE}$ = 494 nm, $\Phi_{F,\ TTPE}$ = 100%, solid film), pronounced AIE characteristic (α_{AIE} = 154), and evident mechanochromic property. But the emission color and aggregation behaviors of these TPE oligomers cannot be tuned by simply extending the chain length. By aid of strong electron-withdrawing cyano groups, which are used to replace the two free phenyls on the central TPE moiety of TTPE, the derivative BTPEFN shows evidently narrowed energy gap ($E_{g,\ BTPEFN}$ = 2.66 eV vs. $E_{g,\ TTPE}$ = 3.08 eV), pronouncedly red-shifted emission ($\lambda_{em,\ BTPEFN}$ = 575 nm, solid film), unity PL quantum efficiency ($\Phi_{F,\ BTPEFN}$ = 100%), and conspicuous aggregation induced emission enhancement (α_{AEE} = 13). By attaching four strong electron-donating *N*,*N*-diethylamino groups onto the peripheral four phenyls of a BTPEFN molecule, the derivative BATPEFN is bestowed with a further narrowed energy gap ($E_{g,\ BATPEFN}$ = 2.15 eV vs. $E_{g,\ TTPE}$ = 3.08 eV) and batho-shifted emission to the infrared region ($\lambda_{em,\ BATPEFN}$ = 713 nm, solid film).

It is noticeable that the intentional introduction of cyano groups into the TPE derivatives has also led to strong ICT,

dx.doi.org/10.1021/jp311360p | J. Phys. Chem. C 2013, 117, 7334–7347

pronounced solvent effect on fluorescence, mechanochromic property, and distinct self-assembling behaviors. The ICT process lowers the PL quantum efficiency of BTPEFN in polar solvents, only Φ_F = 3.4% has been recorded for its THF solution. Moreover, upon the synergetic interaction of the D (*N*,*N*-diethylamino) and A (cyano) moieties, BATPEFN shows an enhanced ICT process, which considerably quenches its fluorescence and makes it impossible to evaluate its AIE characteristic. Owing to the D−A interaction, both BATPEFN and BTPEFN exhibit a conspicuous positive solvatochromism. The emission color of BTPEFN can be tuned from green to red-orange by changing the solvent from apolar (hexane) to polar (THF), while that of BATPEFN can be tuned from red to infrared by tuning in the same series of solvent polarity. BTPEFN demonstrates a unique mechanochromic behavior. The as-prepared solid and the ground powder emit yellow (541 nm) and orange (563 nm) light, respectively. The mechanochromic behavior is reversible by simply repeating the grinding-thermal annealing or grinding-vapor fuming processes. XRD measurement reveals this mechanochromism is driven by the morphology transition between amorphous powder and ordered microcrystals. As to TTPE, the ground powder emits green light (505 nm) and the vapor-fumed sample emits blue light (472 nm). This process is reversible upon repeating the grinding-vapor fuming treatment but insensitive to thermal annealing. The less reversibility of the mechanochromism for TTPE suggests that cyano groups take a crucial part in the related circumstance. Moreover, the cyano groups endow BTPEFN with self-assemble ability and microscaled regular ribbons with bright green fluorescence are obtained in THF/water mixtures of proper water fractions. In contrast, the aggregates formed in TTPE THF/water mixtures are much smaller and much less regular in shape. These results indicate that it is an effective strategy to tune the electronic structure and material property of TPE derivatives in a large range by decorating them with D and A moieties. Through rational molecular design, novel and advanced photonic/electronic materials can be derived and these materials may find versatile applications in high-tech areas.

EXPERIMENTAL SECTION

Materials and Measurements. THF was distilled under normal pressure from sodium benzophenone ketyl under nitrogen immediately prior to use. All chemicals were purchased from Acros or Aldrich and used as received. ^{1}H and ^{13}C NMR spectra were measured on a Mercury plus 400 MHz NMR spectrometer in $CDCl_3$ with tetramethylsilane (TMS; δ = 0 ppm) as internal standard. Elemental analysis was performed on a ThermoFinnigan Flash EA1112 apparatus. MALDI−TOF mass spectra were recorded on a GCT premier CAB048 mass spectrometer. PL spectra were recorded on a spectrofluorophotometer (RF−5301PC, SHIMADZU, Japan). UV absorption spectra were taken on a Varian CARY 100 Bio spectrophotometer. Scanning electron microscope (SEM) images were taken on a S4800 (Hitachi, Japan) scanning electron microscope. Fluorescent images were taken with a Zeiss Axiovert 200 inverted microscope equipped with a 100× oil immersion objective with a numerical aperture of 1.4 and an Ebq 100 Isolated electronic ballast for mercury vapor compressed-arc lamps. TGA spectra were recorded on a DSCQ 1000 (TA, USA) calorimeter. DSC spectra were taken on a Q100 differential scanning calorimeter (TA, USA). XRD patterns were recorded on X'pert PRO, PANalytical, with Cu Kα radiation operating at 40 kV and 40 mA. Cyclic voltammetry was performed at room temperature in a three-electrode cell with use of a CHI-600 Electrochemical Workstation. The ground-state geometries were optimized with the B3LYP/6-31G(d) program, using the Gaussian 03 package.[49] Relative Φ_F values were estimated by using quinine sulfate in 0.1 N sulfuric acid (Φ_F = 54.6%) or rhodamine B in ethanol (Φ_F = 70%) as standards. The absorbance of the solution was kept at ∼0.05 to avoid internal filter effect. Absolute Φ_F values were determined by a calibrated integrating sphere with a diameter of 4 in. (Labsphere Inc.).

Preparation of Aggregates. A stock solution of luminogen in THF with a concentration of 1 mM was prepared. An aliquot (0.1 mL) of the stock solution was transferred to a 10 mL volumetric flask. After the appropriate amount of THF was added, water was added dropwise under vigorous stirring to furnish 10 μM solution with different fractions of water (f_w = 0−99 vol %). The absorption and PL measurements of the resultant solutions were performed immediately.

Synthesis of 1,2-Bis(4-bromophenyl)-1,2-diphenylethene (2). Zinc dust (3.92 g, 60 mmol) was added into a 250-mL two-necked round-bottomed flask. The flask was degassed and flushed with dry nitrogen three times, after which THF (60 mL) was injected. The mixture was cooled to −5 to 0 °C by an ice-salt bath, then titanium tetrachloride (3.32 mL, 30 mmol) was added slowly. The mixture was allowed to warm to 25 °C and kept there for 0.5 h and then refluxed at 74 °C for 2 h. The mixture was cooled to −5 to 0 °C again, treated with 0.5 mL of pyridine, and stirred for 10 min. Then a THF solution (20 mL) of 4-bromophenone (**1**, 5.22 g, 20 mmol) was added slowly. After refluxing overnight, the reaction was quenched with a 10% potassium carbonate aqueous solution and extracted with DCM. The organic layer was washed with brine and dried over anhydrous sodium sulfate. After filtration and solvent evaporation, the residue was purified by silica gel column chromatography, using petroleum ether as eluent. **2** (4.0 g) was obtained as a white solid in 81.6% yield. ^{1}H NMR (400 MHz, $CDCl_3$) δ 7.25−7.19 (m, 4H; Ar H), 7.13−7.07 (m, 6H; Ar H), 7.03−6.96 (m, 4H; Ar H), 6.89−6.85 (m, 4H; Ar H). ^{13}C NMR (100 MHz, $CDCl_3$) δ 143.74, 143.61, 143.29, 143.17, 141.12, 133.62, 131.86, 131.76, 131.56, 128.72, 128.53, 128.41, 127.65, 127.53, 127.35, 121.38, 121.23. For more characterization data, see our previous work.[41]

Synthesis of 1-(4-Bromophenyl)-1,2,2-triphenylethene (3). **3** was synthesized according to Rathore's method.[57] Compound **3** was obtained as a white solid in 87.3% total yield. ^{1}H NMR (400 MHz, $CDCl_3$) δ 7.22 (d, 2H; Ar H), 7.08−7.13 (m, 9H; Ar H), 6.99−7.03 (m, 6H; Ar H), 6.89 (d, 2H; Ar H). ^{13}C NMR (100 MHz, $CDCl_3$) δ 143.48, 143.40, 143.29, 142.76, 141.68, 139.73, 133.06, 131.37, 131.31, 131.29, 130.94, 127.96, 127.87, 127.77, 126.79, 126.73, 126.68, 120.54. For more characterization data, see our previous work.[41]

Synthesis of 4-(1,2,2-Triphenylvinyl)phenylboronic Acid, Pinacol Ester (4). *N*-Butyllithium (1.6 M in hexane, 3.4 mL, 5.5 mmol) was added dropwise into a THF solution (60 mL) of compound **3** (2.1 g, 5 mmol) at −78 °C under nitrogen. After the solution was stirred for 1 h, 2-isopropoxy-4,4,5,5-tetramethyl-1,3,2-dioxaborolane (1.2 mL, 5.5 mmol) was added into the solution slowly. Then the mixture was warmed to 25 °C. After being stirred for 4 h, the mixture was quenched with saturated ammonium chloride solution and extracted with DCM. The organic layer was washed with brine

dx.doi.org/10.1021/jp311360p | J. Phys. Chem. C 2013, 117, 7334−7347

and dried over anhydrous sodium sulfate. After filtration and solvent evaporation, the residue was purified by silica gel column chromatography, using petroleum ether/ethyl acetate (30:1 by volume) as eluent. **4** (1.8 g) was obtained as a white solid in 81.0% yield. ^{1}H NMR (400 MHz, $CDCl_3$) δ 7.66 (d, 2H; Ar H), 7.18−7.09 (m, 17H; Ar H), 1.40 (s, 12H; CH_3). ^{13}C NMR (100 MHz, $CDCl_3$) δ 146.83, 143.73, 143.64, 143.56, 141.45, 140.90, 134.18, 131.39, 131.35, 130.74, 127.78, 127.69, 126.59, 126.51, 83.69, 24.97. For more characterization data, see our previous work.[41]

Synthesis of 1-(4-Bromophenyl)-1-phenyl-2,2-bis(4-diethylamino)phenylethene (6). Compound **6** was synthesized from 4-bromophenone (**1**, 0.8 g, 3.1 mmol), 4,4′-bis (diethylamino)benzophenone (**5**, 1 g, 3.1 mmol), zinc dust (1.21 g, 18.6 mmol), and distilled THF (80 mL). The procedure was similar to that used for compound **2** described above, and 0.96 g of **6** was obtained as a yellow solid in 56.0% yield. ^{1}H NMR (400 MHz, $CDCl_3$) δ 7.19−7.17 (d, 2H; Ar H), 7.10−6.82 (m, 11H, Ar H), 6.41−6.36 (m, 4H, Ar H), 3.32−3.24 (m, 8H; CH_2), 1.14−1.08 (m, 12H; CH_3). ^{13}C NMR (100 MHz, $CDCl_3$) δ 146.43, 145.07, 144.62, 142.26, 133.26, 132.82, 132.77, 131.55, 130.62, 127.62, 125.52, 119.10, 110.83, 110.72, 44.18, 12.63. ESI-MS (m/e) $[MH]^+$ calcd 552.2, found 553.6. Anal. Calcd for $C_{34}H_{37}BrN_2$: C, 73.77, H, 6.74, N, 5.06. Found: C, 74.47, H, 6.90, N, 4.94.

Synthesis of 1-(4-(4,4,5,5-Tetramethyl-1,3,2-dioxaborolan-2-yl)phenyl)-1-phenyl-2,2-bis(4-diethylamino)-phenylethene (7). Compound **7** was synthesized from compound **6** (1.66 g, 3 mmol), *N*-butyllithium (1.6 M in hexane, 2.1 mL, 3.3 mmol), 2-isopropoxy-4,4,5,5-tetramethyl-1,3,2-dioxaborolane (0.7 mL, 3.3 mmol), and THF (40 mL). The procedure was similar to that used for compound **4** described above, and 1.4 g of **7** was obtained as a light yellow solid in 78.0% yield. ^{1}H NMR (400 MHz, $CDCl_3$) δ 7.56 (d, 2H; Ar H), 7.12−7.04 (m, 7H; Ar H), 6.89 (d, 4H; Ar H), 6.42 (d, 4H; Ar H), 3.32−3.28 (m, 8H; CH_2), 1.34 (s, 12H; CH_3), 1.16−1.11 (m, 12H; CH_3). ^{13}C NMR (100 MHz, $CDCl_3$) δ 148.81, 146.35, 145.38, 142.11, 135.95, 133.95, 132.80, 131.61, 130.98, 127.46, 125.31, 110.74, 83.49, 44.13, 24.88, 12.63. ESI-MS (m/e) $[MH]^+$ calcd 600.4, found 601.2. Anal. Calcd for $C_{40}H_{49}BN_2O_2$: C, 79.99, H, 8.22, N, 4.66. Found: C, 80.25, H, 8.33, N, 4.68.

Synthesis of Bis(4-bromophenyl)fumaronitrile (9). Compound **9** was synthesized according to Chen's method,[58] and the product was obtained as an off-white solid in 90% yield. ^{1}H NMR (400 MHz, $CDCl_3$) δ 7.694 (m, 8H; Ar H). ^{13}C NMR (100 MHz, $CDCl_3$) δ 132.654, 130.542, 130.062, 126.763, 124.597, 116.055. For more characterization data, see our previous work.[59]

Synthesis of 1,2-Diphenyl-1,2-bis(4′-(1,2,2-triphenylethenyl)biphenyl-4-yl)ethene (TTPE). Compound **2** (0.74 g, 1.5 mmol), compound **4** (1.5 g, 3.3 mmol), and $Pd(PPh_3)_4$ (76 mg, 2%) were added to a 100-mL two-necked round-bottomed flask. The flask was evacuated under vacuum and flushed with dry nitrogen three times. THF (10 mL) and potassium carbonate solution (2 M, 5 mL) were injected into the flask and the mixture was refluxed overnight. The solution was poured into water and extracted with DCM. The organic layer was washed with brine and dried over sodium sulfate. After filtration and solvent evaporation, the residue was purified by silica gel column chromatography, using chloroform/hexane (2:1 by volume) as eluent. TTPE (0.8 g) was obtained as a light green solid in 54% yield. Mp 337 °C. ^{1}H NMR (400 MHz, $CDCl_3$) δ 7.35−7.31 (m, 8H; Ar H), 7.15−7.04 (m, 48H; Ar H). ^{13}C NMR (100 MHz, $CDCl_3$) δ 143.98, 143.95, 143.93, 142.99, 142.94, 141.24, 140.83, 140.73, 138.51, 138.43, 138.40, 131.98, 131.64, 131.55, 127.97, 127.87, 127.84, 126.75, 126.68, 126.63, 126.22, 126.11. HRMS (MALDI-TOF, m/e) $[M]^+$ calcd for 992.4382, found 992.4376. Anal. Calcd for $C_{78}H_{56}$: C, 94.32, H, 5.68. Found: C, 93.90, H, 5.86.

Synthesis of BTPEFN and BATPEFN. BTPEFN and BATPEFN were prepared by similar synthetic procedures and their characterization data are given here.

2,3-Bis(4′-(1,2,2-triphenylethenyl)biphenyl-4-yl)-fumaronitrile (BTPEFN): BTPEFN (1.1 g) was obtained as a bright yellow solid in 70.4% yield. Mp 247, 288 °C. ^{1}H NMR (400 MHz, $CDCl_3$) δ 7.89 (d, 4H; Ar H), 7.71 (d, 4H; Ar H), 7.40 (d, 4H; Ar H), 7.14−7.03 (m, 34H; Ar H). ^{13}C NMR (100 MHz, $CDCl_3$) δ 144.09, 143.95, 143.52, 143.48, 141.61, 140.19, 136.98, 132.01, 131.49, 131.35, 131.29, 130.70, 129.14, 128.15, 127.80, 127.74, 127.63, 127.42, 126.63, 126.56, 126.50, 126.29, 124.28, 116.84. HRMS (MALDI-TOF, m/e) $[M]^+$ calcd for 890.3661, found 890.3651. Anal. Calcd for $C_{68}H_{46}N_2$: C, 91.65, H, 5.20, N, 3.14. Found: C, 90.99, H, 5.11, N, 3.17.

2,3-Bis(4′-(2,2-bis(4-(diethylamino)phenyl)-1-phenylethenyl)-biphenyl-4-yl)fumaronitrile (BATPEFN): BATPEFN (0.82 g) was obtained as a black solid in 87.2% yield. ^{1}H NMR (400 MHz, $CDCl_3$) δ 7.90 (d, 4H; Ar H), 7.73 (d, 4H; Ar H), 7.41 (d, 4H; Ar H), 7.16−7.08 (m, 14H; Ar H), 6.93−6.90 (m, 8H; Ar H), 6.44−6.40 (m, 8H; Ar H), 3.33−3.27 (m, 16H; CH_2), 1.15−1.10 (m, 24H; CH_3). ^{13}C NMR (100 MHz, $CDCl_3$) δ 146.52, 146.38, 146.15, 145.32, 144.30, 142.38, 135.72, 132.87, 132.25, 131.65, 130.45, 129.11, 127.62, 127.26, 126.12, 125.48, 124.09, 116.99, 110.82, 110.73, 44.17, 12.61. HRMS (MALDI-TOF, m/e) $[M]^+$ calcd for 1174.6601, found 1174.6641. Anal. Calcd for $C_{84}H_{82}N_6$: C, 85.82, H, 7.03, N, 7.15. Found: C, 85.44, H, 7.16, N, 6.88.

■ ASSOCIATED CONTENT

Supporting Information

Mass spectra (Figures S1−S3); thermal gravity analysis (DSC and TGA curve, Figures S4 and S5); UV−vis spectra in dilute THF (Figure S6); AIE properties of TTPE (Figure S7); UV−vis spectra of BTPEFN in THF/water mixtures (Figure S8); UV−vis absorption spectra of BTPEFN and BATPEFN in different solvents (Figure S9); solvent effect of TTPE (Figure S10); plot of Stokes shift ($\Delta\upsilon$) versus Δf (Figure S11); cyclic voltammograms (Figure S12); XRD pattern of BTPEFN aggregates formed in the THF/water mixture of BDABFN formed from THF/water mixtures (Figure S13); SEM and fluorescence microscope images of BTPEFN formed from THF/water mixtures (Figure S14); the electron diffraction pattern of the aggregates of TTPE formed in a THF/water mixture with f_w = 60% (Figure S15); XRD patterns of TTPE solids obtained in different conditions (Figure S16); and optical transitions of BTPEFN, BATPEFN, and TTPE in different solvents (Table S1). This material is available free of charge via the Internet at http://pubs.acs.org.

■ AUTHOR INFORMATION

Corresponding Author

*Tel: +86-571-87953734 (J.Z.S.) and +852-2358-7375 (B.Z.T.). Fax: +86-571-87953734 (J.Z.S.) and +852-2358-1594 (B.Z.T.). E-mail: sunjz@zju.edu.cn (J.Z.S.) and tangbenz@ust.hk (B.Z.T.).

Notes

The authors declare no competing financial interest.

■ ACKNOWLEDGMENTS

This work was supported partly by the Natural National Science Foundation of China (51273175), the Ministry of Science and Technology of China (2013CB834704), the Natural Science Foundation of Zhejiang Province (Z4110056), the Research Grants Council of Hong Kong (603509, HKUST2/CRF/10, and N_HKUST620/11), and the University Grants Committee of Hong Kong (AoE/P-03/08).

■ REFERENCES

(1) Tang, C. W.; VanSlyke, S. A. Organic Electroluminescent Diodes. *Appl. Phys. Lett.* **1987**, *51*, 913−915.
(2) Wu, C. C.; Lin, Y. T.; Wong, K. T.; Chen, R. T.; Chien, Y. Y. Efficient Organic Blue-Light-Emitting Devices with Double Confinement on Terfluorenes with Ambipolar Carrier Transport Properties. *Adv. Mater.* **2004**, *16*, 61−65.
(3) Wu, K. C.; Ku, P. J.; Lin, C. S.; Shih, H. T.; Wu, F. I.; Huang, M. J.; Lin, J. J.; Chen, I. C.; Cheng, C. H. The Photophysical Properties of Dipyrenylbenzenes and Their Application as Exceedingly Efficient Blue Emitters for Electroluminescent Devices. *Adv. Funct. Mater.* **2008**, *18*, 67−75.
(4) Grimsdale, A. C.; Chan, K. L.; Martin, R. E.; Jokisz, P. G.; Holmes, A. B. Synthesis of Light-Emitting Conjugated Polymers for Applications in Electroluminescent Devices. *Chem. Rev.* **2009**, *109*, 897−1091.
(5) Yeh, H.-C.; Chan, L.-H.; Wu, W.-C.; Chen, C.-T. Non-doped Red Organic Light-Emitting Diodes. *J. Mater. Chem.* **2004**, *14*, 1293−1298.
(6) Birks, J. B. *Photophysics of Aromatic Molecules*; Wiley: London, UK, 1970.
(7) Yeh, H.-C.; Yeh, S.-J.; Chen, C.-T. Readily Synthesised Arylamino Fumaronitrile for Non-doped Red Organic Light-Emitting Diodes. *Chem. Commun.* **2003**, 2632−2633.
(8) Chiang, C.-L.; Tseng, S.-M.; Chen, C.-T.; Hsu, C.-P.; Shu, C.-F. Influence of Molecular Dipoles on the Photoluminescence and Electroluminescence of Dipolar Spirobifluorenes. *Adv. Funct. Mater.* **2008**, *18*, 248−257.
(9) Wang, J.; Zhao, Y.; Dou, C.; Sun, H.; Xu, P.; Ye, K.; Zhang, J.; Jiang, S.; Li, F.; Wang, Y. Alkyl and Dendron Substituted Quinacridones: Synthesis, Structures, and Luminescent Properties. *J. Phys. Chem. B* **2007**, *111*, 5082−5089.
(10) Lee, S. H.; Jang, B.-B.; Kafafi, Z. H. Highly Fluorescent Solid-State Asymmetric Spirosilabifluorene Derivatives. *J. Am. Chem. Soc.* **2005**, *127*, 9071−9078.
(11) Luo, J.; Xie, Z.; Lam, J. W. Y.; Cheng, L.; Chen, H.; Qiu, C.; Kwok, H. S.; Zhan, X.; Liu, Y.; Zhu, D.; et al. Aggregation-Induced Emission of 1-Methyl-1,2,3,4,5-pentaphenylsilole. *Chem. Commun.* **2001**, 1740−1741.
(12) Chen, J.; Law, C. C. W.; Lam, J. W. Y.; Dong, Y.; Lo, S. M. F.; Williams, I. D.; Zhu, D.; Tang, B. Z. Synthesis, Light Emission, Nanoaggregation, and Restricted Intramolecular Rotation of 1,1-Substituted 2,3,4,5-Tetraphenylsiloles. *Chem. Mater.* **2003**, *15*, 1535−1546.
(13) Qin, A.; Lam, J. W. Y.; Tang, B. Z. Luminogenic Polymers with Aggregation-Induced Emission Characteristics. *Prog. Polym. Sci.* **2012**, *37*, 182−209.
(14) Hong, Y.; Lam, J. W. Y.; Tang, B. Z. Aggregation-Induced Emission. *Chem. Soc. Rev.* **2011**, *40*, 5361−5388.
(15) Zhang, S.; Qin, A.; Sun, J. Z.; Tang, B. Z. Mechanism Study of Aggregation-Induced Emission Progress in Chemistry. *Prog. Chem.* **2011**, *23*, 623−636.
(16) Zhao, Z.; Lam, J. W. Y.; Tang, B. Z. Aggregation-Induced Emission of Tetraarylethene Luminogens. *Curr. Org. Chem.* **2010**, *14*, 2109−2132.
(17) Wang, M.; Zhang, G.; Zhang, D.; Zhu, D.; Tang, B. Z. Fluorescent Bio/chemosensors Based on Silole and Tetraphenylethene Luminogens with Aggregation-Induced Emission Feature. *J. Mater. Chem.* **2010**, *20*, 1858−1867.
(18) Wang, J.; Mei, J.; Hu, R.; Sun, J. Z.; Qin, A.; Tang, B. Z. Click Synthesis, Aggregation-Induced Emission, E/Z Isomerization, Self-Organization, and Multiple Chromisms of Pure Stereoisomers of a Tetraphenylethene-Cored Luminogen. *J. Am. Chem. Soc.* **2012**, *134*, 9956−9966.
(19) Yuan, W. Z.; Gong, Y.; Chen, S.; Shen, X. Y.; Lam, J. W. Y.; Lu, P.; Lu, Y.; Wang, Z.; Hu, R.; Xie, N.; et al. Efficient Solid Emitters with Aggregation-Induced Emission and Intramolecular Charge Transfer Characteristics: Molecular Design, Synthesis, Photophysical Behaviors, and OLED Application. *Chem. Mater.* **2012**, *24*, 1518−1528.
(20) Hong, Y.; Meng, L.; Chen, S.; Leung, C. W. T.; Da, L. T.; Faisal, M.; Silva, D. A.; Liu, J.; Lam, J. W. Y.; Huang, X.; et al. Monitoring and Inhibition of Insulin Fibrillation by a Small Organic Fluorogen with Aggregation-Induced Emission Characteristics. *J. Am. Chem. Soc.* **2012**, *134*, 1680−1689.
(21) Zhao, Z.; Geng, J.; Chang, Z.; Chen, S.; Deng, C.; Jiang, T.; Qin, W.; Lam, J. W. Y.; Kwok, H. S.; Qiu, H.; et al. A Tetraphenylethene-Based Red Luminophor for An Efficient Non-doped Electroluminescence Device and Cellular Imaging. *J. Mater. Chem.* **2012**, *22*, 11018−11021.
(22) Zhao, Q.; Zhang, S.; Liu, Y.; Mei, J.; Chen, S. J.; Lu, P.; Qin, A.; Ma, Y.; Sun, J. Z.; Tang, B. Z. Tetraphenylethenyl-Modified Perylene Bisimide: Aggregation-Induced Red Emission, Electrochemical Properties and Ordered Microstructures. *J. Mater. Chem.* **2012**, *22*, 7387−7394.
(23) Du, X. B.; Qi, J.; Zhang, Z. Q.; Ma, D. G.; Wang, Z. Y. Efficient Non-doped Near Infrared Organic Light-Emitting Devices Based on Fluorophores with Aggregation-Induced Emission Enhancement. *Chem. Mater.* **2012**, *24*, 2178−2185.
(24) Chi, Z.; Zhang, X.; Xu, B.; Zhou, X.; Ma, C.; Zhang, Y.; Liu, S.; Xu, J. Recent Advances in Organic Mechanofluorochromic Materials. *Chem. Soc. Rev.* **2012**, *41*, 3878−3896.
(25) Li, H.; Chi, Z.; Xu, B.; Zhang, X.; Li, X.; Liu, S.; Zhang, Y.; Xu, J. Aggregation-Induced Emission Enhancement Compounds Containing Triphenylamine-Anthrylenevinylene and Tetraphenylethene Moieties. *J. Mater. Chem.* **2011**, *21*, 3760−3767.
(26) Bhalla, V.; Vij, V.; Dhir, A.; Kumar, M. Hetero-oligophenylene-Based AIEE Material as A Multiple Probe for Biomolecules and Metal Ions to Construct Logic Circuits: Application in Bioelectronics and Chemionics. *Chem.—Eur. J.* **2012**, *18*, 3765−3772.
(27) Aldred, M. P.; Li, C.; Zhang, G. F.; Gong, W. L.; Li, A. D. Q.; Dai, Y. F.; Ma, D. G.; Zhu, M. Q. Fluorescence Quenching and Enhancement of Vitrifiable Oligofluorenes End-Capped with Tetraphenylethene. *J. Mater. Chem.* **2012**, *22*, 7515−7528.
(28) Wang, X. R.; Hu, J. M.; Liu, T.; Zhang, G.; Liu, S. Highly Sensitive and Selective Fluorometric Off−On K^+ Probe Constructed via Host−Guest Molecular Recognition and Aggregation-Induced Emission. *J. Mater. Chem.* **2012**, *22*, 8622−8628.
(29) Shustova, N. B.; Ong, T.-C.; Cozzolino, A. F.; Michaelis, V. K.; Griffin, R. G.; Dinca, M. Phenyl Ring Dynamics in a Tetraphenylethylene-Bridged Metal-Organic Framework: Implications for the Mechanism of Aggregation-Induced Emission. *J. Am. Chem. Soc.* **2012**, *134*, 15061−15070.
(30) Shustova, N. B.; McCarthy, B. D.; Dinca, M. Turn-On Fluorescence in Tetraphenylethylene-Based Metal-Organic Frameworks: An Alternative to Aggregation-Induced Emission. *J. Am. Chem. Soc.* **2011**, *133*, 20126−20129.
(31) Kapadia, P. P.; Ditzler, L. R.; Baltrusaitis, J.; Swenson, D. C.; Tivanski, A. V.; Pigge, F. C. Semiconducting Organic Assemblies Prepared from Tetraphenylethylene Tetracarboxylic Acid and Bis(pyridine)s via Charge-Assisted Hydrogen Bonding. *J. Am. Chem. Soc.* **2011**, *133*, 8490−8493.
(32) Sun, F.; Zhang, G.; Zhang, D.; Xue, L.; Jiang, H. Aqueous Fluorescence Turn-on Sensor for Zn^{2+} with a Tetraphenylethylene Compound. *Org. Lett.* **2011**, *13*, 6378−6381.

(33) Xu, B.; Chi, Z.; Li, H.; Zhang, X.; Li, X.; Liu, S.; Zhang, Y.; Xu, J. Synthesis and Properties of Aggregation-Induced Emission Compounds Containing Triphenylethene and Tetraphenylethene Moieties. *J. Phys. Chem. C* **2011**, *115*, 17574−17581.
(34) Liu, Y.; Qin, A.; Chen, X.; Shen, X. Y.; Tong, L.; Hu, R.; Sun, J. Z.; Tang, B. Z. Specific Recognition of β-Cyclodextrin by A Tetraphenylethene Luminogen through A Cooperative Boronic Acid/Diol Interaction. *Chem.—Eur. J.* **2011**, *17*, 14736−14740.
(35) Weil, T.; Vosch, T.; Hofkens, J.; Peneva, K.; Müellen, K. The Rylene Colorant Family−Tailored Nanoemitters for Photonics Research and Applications. *Angew. Chem., Int. Ed.* **2010**, *49*, 9068−9093.
(36) Zhan, X.; Facchetti, A.; Barlow, S.; Marks, T. J.; Ratner, M. A.; Wasielewski, M. R.; Marder, S. R. Rylene and Related Diimides for Organic Electronics. *Adv. Mater.* **2011**, *23*, 268−284.
(37) Tang, C. W.; VanSlyke, S. A.; Chen, C. H. Electroluminescence of Doped Organic Thin Films. *J. Appl. Phys.* **1989**, *65*, 3610−3616.
(38) Mei, J.; Wang, J.; Sun, J. Z.; Zhao, H.; Yuan, W. Z.; Deng, C.; Chen, S.; Sung, H. H. Y.; Lu, P.; Qin, A.; et al. Siloles Symmetrically Substituted on Their 2,5-Positions with Electron-Accepting and Donating Moieties: Facile Synthesis, Aggregation-Enhanced Emission, Solvatochromism, and Device Application. *Chem. Sci.* **2012**, *3*, 549−558.
(39) Mei, J.; Wang, J.; Qin, A.; Zhao, H.; Yuan, W. Z.; Zhao, Z.; Sung, H. H. Y.; Deng, C.; Zhang, S.; Williams, I. D.; et al. Construction of Soft Porous Crystal with Silole Derivative: Strategy of Framework Design, Multiple Structural Transformability and Mechanofluorochromism. *J. Mater. Chem.* **2012**, *22*, 4290−4298.
(40) Shen, X. Y.; Yuan, W. Z.; Liu, Y.; Zhao, Q.; Lu, P.; Ma, Y.; Williams, I. D.; Qin, A.; Sun, J. Z.; Tang, B. Z. Fumaronitrile-Based Fluorogen: Red to Near-Infrared Fluorescence, Aggregation-Induced Emission, Solvatochromism, and Twisted Intramolecular Charge Transfer. *J. Phys. Chem. C* **2012**, *116*, 10541−10547.
(41) Hu, R.; Maldonado, J. L.; Rodriguez, M.; Deng, C.; Jim, C. K. W.; Lam, J. W. Y.; Yuen, M. M. F.; Ramos-Ortiz, G.; Tang, B. Z. Luminogenic Materials Constructed from Tetraphenylethene Building Blocks: Synthesis, Aggregation-Induced Emission, Two-Photon Absorption, Light Refraction, and Explosive Detection. *J. Mater. Chem.* **2012**, *22*, 232−240.
(42) Zhao, Z.; Chen, S.; Lam, J. W. Y.; Jim, C. K. W.; Chan, C. Y. K.; Wang, Z.; Lu, P.; Deng, C.; Kwok, H. S.; Ma, Y.; et al. Steric Hindrance, Electronic Communication, and Energy Transfer in the Photo- and Electroluminescence Processes of Aggregation-Induced Emission Luminogens. *J. Phys. Chem. C* **2010**, *114*, 7963−7972.
(43) Dong, Y.; Lam, J. W. Y.; Qin, A.; Liu, J.; Li, Z.; Tang, B. Z.; Sun, J. Z.; Kwok, H. S. Aggregation-Induced Emissions of Tetraphenylethene Derivatives and Their Utilities as Chemical Vapor Sensors and in Organic Light-Emitting Diodes. *Appl. Phys. Lett.* **2007**, *91*, 011111−011113.
(44) Zhao, Z.; Chen, S.; Shen, X. Y.; Mahtab, F.; Yu, Y.; Lu, P.; Lam, J. W. Y.; Kwok, H. S.; Tang, B. Z. Aggregation-Induced Emission, Self-Assembly, and Electroluminescence of 4,4′-Bis(1,2,2-triphenylvinyl)-biphenyl. *Chem. Commun.* **2010**, 686−688.
(45) Auweter, H.; Haberkorn, H.; Heckmann, W.; Horn, D.; Lüddecke, E.; Rieger, J.; Weiss, H. Supramolecular Structure of Precipitated Nanosize β-Carotene Particles. *Angew. Chem., Int. Ed.* **1999**, *38*, 2188−2191.
(46) Lippert, E. *Z. Naturforsch., A: Phys. Sci.* **1955**, *10*, 541−545.
(47) Mataga, N.; Kaifu, Y.; Koizumi, M. *Bull. Chem. Soc. Jpn.* **1956**, *29*, 465−470.
(48) Wojtyk, J. T. C.; Wasey, A.; Kazmaier, P. M.; Hoz, S.; Buncel, E. Thermal Reversion Mechanism of N-Functionalized Merocyanines to Spiropyrans: A Solvatochromic, Solvatokinetic, and Semiempirical Study. *J. Phys. Chem. A* **2000**, *104*, 9046−9055.
(49) Frisch, M. J.; Trucks, G. W.; Schlegel, H. B.; Scuseria, G. E.; Robb, M. A.; Cheeseman, J. R.; Montgomery, J. A., Jr.; Vreven, T.; Kudin, K. N.; Burant, J. C. et al. *Gaussian 03*, Revision E.01; Gaussian, Inc.: Wallingford, CT, 2004.
(50) Li, Y.; Cao, Y.; Gao, J.; Wang, D.; Yu, G.; Heeger, A. Electrochemical Properties of Luminescent Polymers and Polymer Light-Emitting Electrochemical Cells. *J. Synth. Met.* **1999**, *99*, 243−248.
(51) An, B. K.; Gihm, S. H.; Chuang, J. W.; Park, C. R.; Kwon, S. K.; Park, S. Y. Color-Tuned Highly Fluorescent Organic Nanowires/Nanofabrics: Easy Massive Fabrication and Molecular Structural Origin. *J. Am. Chem. Soc.* **2009**, *131*, 3950−3957.
(52) Liu, H.; Xu, J.; Li, Y.; Li, Y. Aggregate Nanostructures of Organic Molecular Materials. *Acc. Chem. Res.* **2010**, *43*, 1496−1508.
(53) Dou, C.; Han, L.; Zhao, S.; Zhang, H.; Wang, Y. Multi-Stimuli-Responsive Fluorescence Switching of a Donor-Acceptor π-Conjugated Compound. *J. Phys. Chem. Lett.* **2011**, *2*, 666−670.
(54) Yoon, S. J.; Park, S. Y. Polymorphic and Mechanochromic Luminescence Modulation in the Highly Emissive Dicyanodistyrylbenzene Crystal: Secondary Bonding Interaction in Molecular Stacking Assembly. *J. Mater. Chem.* **2011**, *21*, 8338−8346.
(55) Luo, X.; Zhao, W.; Shi, J.; Li, C.; Liu, Z.; Bo, Z.; Dong, Y. Q.; Tang, B. Z. Reversible Switching Emissions of Tetraphenylethene Derivatives among Multiple Colors with Solvent Vapor, Mechanical, and Thermal Stimuli. *J. Phys. Chem. C* **2012**, *116*, 21967−21972.
(56) Zhang, X.; Chi, Z.; Zhou, X.; Liu, S.; Zhang, Y.; Xu, J. Influence of Carbazolyl Groups on Properties of Piezofluorochromic Aggregation-Enhanced Emission Compounds Containing Distyrylanthracene. *J. Phys. Chem. C* **2012**, *116*, 23629−23638.
(57) Banerjee, M.; Emond, S. J.; Lindeman, S. V.; Rathore, R. Practical Synthesis of Unsymmetrical Tetraarylethylenes and Their Application for the Preparation of [Triphenylethylene−Spacer−Triphenylethylene] Triads. *J. Org. Chem.* **2007**, *72*, 8054−8061.
(58) Yeh, H.-C.; Wu, W.-C.; Wen, Y.-S.; Dai, D.-C.; Wang, J.-K.; Chen, C.-T. Derivative of α,β-Dicyanostilbene: Convenient Precursor for the Synthesis of Diphenylmaleimide Compounds, *E*−*Z* Isomerization, Crystal Structure, and Solid-State Fluorescence. *J. Org. Chem.* **2004**, *69*, 6455−6462.
(59) Li, K.; Qin, W.; Ding, D.; Tomczak, N.; Geng, J.; Liu, R.; Liu, J.; Zhang, X.; Liu, H.; Liu, B.; et al. Photostable Fluorescent Organic Dots with Aggregation-Induced Emission (AIE Dots) for Noninvasive Long-Term Cell Tracing. *Sci. Rep.* **2013**, DOI: 10.1038/srep01150.